ELSEVIER

Engineering Analysis with Boundary Elements 26 (2002) 119–132

ENGINEERING ANALYSIS *with* BOUNDARY ELEMENTS

www.elsevier.com/locate/enganabound

Transient heat conduction in homogeneous and non-homogeneous materials by the Laplace transform Galerkin boundary element method

Alok Sutradhar[a], Glaucio H. Paulino[a,*], L.J. Gray[b]

[a]*Department of Civil and Environmental Engineering, University of Illinois at Urbana-Champaign, 2209 Newmark Laboratory, 205 North Mathews Avenue, Urbana, IL 61801, USA*

[b]*Computer Science and Mathematics Division, Oak Ridge National Laboratory, Building 6012, Oak Ridge, TN 37831, USA*

Received 19 March 2001; revised 30 July 2001; accepted 29 August 2001

Abstract

The Green's function for three-dimensional transient heat conduction (diffusion equation) for functionally graded materials (FGMs) is derived. The thermal conductivity and heat capacitance both vary exponentially in one coordinate. In the process of solving this diffusion problem numerically, a Laplace transform (LT) approach is used to eliminate the dependence on time. The fundamental solution in Laplace space is derived and the boundary integral equation formulation for the Laplace Transform boundary element method (LTBEM) is obtained. The numerical implementation is performed using a Galerkin approximation, and the time-dependence is restored by numerical inversion of the LT. Two numerical inversion techniques have been investigated: a Fourier series method and Stehfest's algorithm, the latter being preferred. A number of test problems have been examined, and the results are in excellent agreement with available analytical solutions.

Keywords: Green's functions; Transient heat conduction; Functionally graded materials; Laplace transform boundary element method; Galerkin approximation

1. Introduction

Transient heat conduction problems can be efficiently solved with the boundary element method (BEM). The various procedures reported in the literature can essentially be classified into two broad categories: (1) the time domain approach and (2) the transform space approach.

In the *time domain approach*, a time marching scheme associated with the BEM solution at each time step is used, and solutions are found directly in the time domain. The time dependent fundamental solution is used to transform the differential system into a boundary integral equation. The numerical solution of the boundary integral requires both space and time discretization. Early works using the time-domain approach include those by Chang et al. [1], Shaw [2], Curran et al. [3], Wrobel and Brebbia [4], and many others. Recent works involve that of Lesnic et al. [5], Coda and Venturini [6,7], Pasquetti and Caruso [8], Wrobel et al. [9], Divo and Kassab [10], etc.

By employing a time-dependent fundamental solution together with recent developments in techniques for converting volume integrals into a (series of) boundary integrals, the diffusion problem can be solved by means of finite-differencing in time and BEM discretization for the spatial variables. The volume integral can be converted through either a set of local interpolation functions — known as the dual reciprocity method, as presented by Brebbia and Wrobel [11] — or a hierarchy of higher order fundamental solutions — known as the multiple reciprocity method, as presented by Nowak [12].

A drawback of time-marching schemes is that they can be numerically inefficient. An alternative is to employ a *transform space* approach, wherein the time dependent derivative is eliminated in favor of a (algebraic) transform variable. However, once the differential system is solved in transform space, reconstituting the solution in the time domain requires an inverse transform. Although this approach is simple and attractive, the accuracy depends upon an efficient and accurate numerical inverse transform. For diffusion problems, LT seems to be the best choice. The first such formulation utilizing the LT approach was proposed by Rizzo and Shippy [13] for solution of heat conduction problems in solids. Later, Liggett and Liu [14] extended the method to unsteady flows in confined aquifers. Early Laplace inversion methods were not efficient, as they employed a type of curve fitting process for which the behavior of the solution had to be known a priori. However,

* Corresponding author. Tel.: +1-217-333-3817; fax: +1-217-265-8041.
E-mail address: paulino@uiuc.edu (G.H. Paulino).

0955-7997/02/$ - see front matter
PII: S0955-7997(01)00090-X

with the advancement of techniques for inverse LT, this approach has received renewed attention. Moridis and Reddell [15] successfully used their Laplace transform boundary element method (LTBEM) for diffusion type problems. Cheng et al. [16] also used the BEM to solve axi-symmetric diffusion problems in the LT space. Zhu et al. [17], Zhu and Satravaha [18], and Zhu [19] extended the work to the Laplace transform dual reciprocity method (LTDRM), for solving non-linear diffusion equations with a source term and temperature-dependent diffusivity. Goldberg and Chen [20] used the Method of fundamental solutions (MFS) in Laplace space for both diffusion and Helmholtz equations. Maillet et al. [24] recently used this approach to solve heat transfer problems by the quadrupole method. Some details of both approaches (i.e. time domain and transformed space) in transient problems can be found in Ref. [19]. Similar problems for different applications have been presented by Cheng [21] for ground water flow in heterogeneous media, and by Wu and Lee [22] and Lacerda et al. [23] for acoustic propagation with a mean flow.

As is usual in boundary element applications, all the above work assumes a homogeneous medium. The present work is concerned with transient heat transfer in functionally graded materials (FGMs); the steady state FGM problem has been examined in Ref. [25]. The composition and the volume fraction of FGM constituents vary gradually, giving a non-uniform microstructure with continuously graded macroproperties (e.g. specific heat, conductivity, density). For instance, one face of a structural component (plate or cylinder) may be an engineering ceramic that can resist severe thermal loading, and the other face may be a metal to maintain structural rigidity and toughness. Example applications include pressure vessels and pipes in nuclear reactors or chemical plants, and other examples can be found in the review papers by Tanigawa [26] and Noda [27]. A comprehensive treatment of the science and technology of FGMs can be found in the book by Suresh and Mortensen [28] or the book by Miyamoto et al. [29].

In this work, the Green's function for the three-dimensional (3D) FGM transient diffusion equation is derived using an exponential variation transform; the boundary integral equation based upon this Green's function is then solved numerically using a Galerkin (as opposed to collocation) approximation [30]. The exponential transform technique has been used earlier by Carslaw and Jaeger [31] to obtain analytical solutions for various problems. Moreover, Li and Evans [32], Onishi and Ikeuchi [33], Ramachandran [34] and, more recently, Singh and Tanaka [35] have used this transform to solve advection–diffusion problems.

The remainder of this paper is organized as follows. The basic equations of the diffusion problem are described in Section 2. The Green's function for the FGM diffusion equation is derived in Section 3. In Section 4, the LTBEM formulation is presented. Section 5 discusses several aspects of the numerical implementation of the boundary integral analysis and Section 6 does the same for the numerical inversion of the LT. Some numerical examples are presented in Section 7. Finally, concluding remarks and directions for future research are discussed in Section 8. In Appendix A, the analytical solution for one of the FGM problems (from Section 7) is given.

2. Basic equations

The transient diffusion equation is given by

$$\nabla\cdot(k\nabla\phi) = c\frac{\partial\phi}{\partial t}, \tag{1}$$

where $\phi = \phi(x, y, z; t)$ is the temperature function, c is the specific heat and k is the thermal conductivity. We assume that the thermal conductivity varies exponentially in one Cartesian coordinate, i.e.

$$k(x, y, z) = k_0 e^{2\beta z}, \tag{2}$$

in which β is the non-homogeneity parameter. The specific heat is also graded with the same functional variation as the conductivity

$$c(x, y, z) = c_0 e^{2\beta z}. \tag{3}$$

Substituting these material expressions in Eq. (1), one obtains

$$\nabla^2\phi + 2\beta\phi_z = \frac{1}{\alpha}\frac{\partial\phi}{\partial t}, \tag{4}$$

where $\alpha = k_0/c_0$ and ϕ_z denotes the derivative of ϕ with respect to z (i.e. $\phi_z \equiv \partial\phi/\partial z$).

Two types of boundary conditions are prescribed. The Dirichlet condition for the unknown potential ϕ is

$$\phi(x, y, z; t) = \bar{\phi}(x, y, z; t), \tag{5}$$

on boundary Σ_1 and the Neumann condition for its flux is

$$q(x, y, z; t) = -k(\cdot)\frac{\partial\phi(x, y, z; t)}{\partial n} = \bar{q}(x, y, z; t), \tag{6}$$

on boundary Σ_2, where $\mathbf{n}$ is the unit outward normal to Σ_2. Here, a bar over the quantity of interest means that it assumes a prescribed value. For a well-posed problem, $\Sigma_1 \cup \Sigma_2 = \Sigma$ with Σ being the entire boundary. As the problem is time dependent, in addition to these boundary conditions, an initial condition at a specific time t_0 must also be prescribed. A zero initial temperature distribution has been considered in all the examples in this paper, i.e.

$$\phi(x, y, z; t_0) = \phi_0(x, y, z) = 0. \tag{7}$$

A non-zero initial temperature distribution may be solved with the dual reciprocity method [36].

3. Green's function

The Green's function for Eq. (4) can be derived by

employing the substitution

$$\phi = \mathrm{e}^{-\beta z-\beta^2\alpha t}u. \tag{8}$$

Thus, the derivatives in Eq. (4) can be expressed in terms of u, as follows

$$\frac{\partial\phi}{\partial z} = -\beta\mathrm{e}^{-\beta z-\beta^2\alpha t}u + \mathrm{e}^{-\beta z-\beta^2\alpha t}\frac{\partial u}{\partial z}, \tag{9}$$

$$\frac{\partial^2\phi}{\partial z^2} = \beta^2\mathrm{e}^{-\beta z-\beta^2\alpha t}u - 2\beta\mathrm{e}^{-\beta z-\beta^2\alpha t}\frac{\partial u}{\partial z} + \mathrm{e}^{-\beta z-\beta^2\alpha t}\frac{\partial^2 u}{\partial z^2}, \tag{10}$$

$$\frac{1}{\alpha}\frac{\partial\phi}{\partial t} = \frac{1}{\alpha}(-\beta^2\alpha\mathrm{e}^{-\beta z-\beta^2\alpha t})u + \frac{\mathrm{e}^{-\beta z-\beta^2\alpha t}}{\alpha}\frac{\partial u}{\partial t}. \tag{11}$$

Substituting Eqs. (9)–(11), in Eq. (4), one obtains

$$\nabla^2 u = \frac{1}{\alpha}\frac{\partial u}{\partial t}, \tag{12}$$

which is the standard diffusion equation for a homogeneous material problem. The time dependent fundamental solution for this equation is known [37], and is given by

$$u^* = \frac{1}{(4\pi\alpha\tau)^{3/2}}\mathrm{e}^{-(r^2/4\alpha\tau)}, \tag{13}$$

where $\tau = t_\mathrm{F} - t$. Note that the function u^* represents the temperature field at time t_F produced by an instantaneous source of heat at point $P(x_p, y_p, z_p)$ and time t. The 3D fundamental solution to the FGM diffusion equation can be written by back substitution (using Eq. (8)) as

$$\phi^* = \frac{1}{(4\pi\alpha\tau)^{3/2}}\mathrm{e}^{-\beta(z-z_p)-\beta^2\alpha\tau-(r^2/4\alpha\tau)}. \tag{14}$$

4. Laplace transform BEM formulation

Let the LT of ϕ be denoted by

$$\tilde{\phi}(Q,s) = \int_{\mathscr{R}} \phi(Q,t)\mathrm{e}^{-st}\,\mathrm{d}t. \tag{15}$$

Thus, in LT space, the differential Eq. (4) becomes

$$\nabla^2\tilde{\phi} + 2\beta\tilde{\phi}_z - \frac{s}{\alpha}\tilde{\phi} = 0, \tag{16}$$

where $\phi_0 = 0$ (at $t = 0$) is considered (see Eq. (7)).

Following the usual practice, the corresponding boundary integral statement can be obtained by 'orthogonalizing' this equation against an arbitrary (for now) function $f(x,y,z) = f(Q)$, i.e. integrating over a bounded volume V

$$\int_V f(Q)\left(\nabla^2\tilde{\phi} + 2\beta\tilde{\phi}_z - \frac{s}{\alpha}\tilde{\phi}\right)\mathrm{d}V_Q = 0. \tag{17}$$

According to Green's second identity, if the two functions ϕ and λ have continuous first and second derivatives in V, then

$$\int_V (\phi\nabla^2\lambda - \lambda\nabla^2\phi)\mathrm{d}V = \int_\Sigma\left(\phi\frac{\partial\lambda}{\partial n} - \lambda\frac{\partial\phi}{\partial n}\right)\mathrm{d}S. \tag{18}$$

Using this relation and denoting the boundary of V by Σ, the first term of Eq. (17) becomes

$$\int_V f(Q)\nabla^2\tilde{\phi}\;\mathrm{d}V_Q = \int_V \tilde{\phi}(Q)\nabla^2 f(Q)\mathrm{d}V_Q + \int_\Sigma\left(f(Q)\frac{\partial}{\partial n}\tilde{\phi}(Q) - \tilde{\phi}(Q)\frac{\partial}{\partial n}f(Q)\right)\mathrm{d}S_Q. \tag{19}$$

Integrating by parts the second term of Eq. (17), we obtain

$$\int_V 2\beta f(Q)\tilde{\phi}_z\,\mathrm{d}V_Q = \int_\Sigma 2\beta f(Q)n_z\tilde{\phi}(Q)\mathrm{d}S_Q - \int_V 2\beta\frac{\partial f}{\partial z}\tilde{\phi}(Q)\mathrm{d}V_Q, \tag{20}$$

and using Eqs. (19) and (20) in Eq. (17), we get after simplification

$$0 = \int_\Sigma\left(f(Q)\frac{\partial}{\partial n}\tilde{\phi}(Q) - \tilde{\phi}(Q)\frac{\partial}{\partial n}f(Q) + 2\beta n_z(Q)\tilde{\phi}(Q)f(Q)\right)\mathrm{d}S_Q + \int_V\tilde{\phi}(Q)\left(\nabla^2 f(Q) - 2\beta f_z(Q) - \frac{s}{\alpha}f(Q)\right)\mathrm{d}V_Q, \tag{21}$$

where $f_z = \partial f/\partial z$, and $\mathbf{n}(Q) = (n_x, n_y, n_z)$ is the unit outward normal on Σ.

If we select $f(Q) = G(P,Q)$ as a Green's function, then the Green's function equation is (cf. Eq. (4))

$$\nabla^2 G(P,Q) - 2\beta G_z(Q) - \frac{s}{\alpha}G(P,Q) = -\delta(Q-P), \tag{22}$$

where δ is the Dirac Delta function. Thus the source point volume integral in Eq. (21) becomes $-\tilde{\phi}(P)$. By means of Eq. (22), Eq. (21) can be rewritten as

$$\tilde{\phi}(P) + \int_\Sigma\left(\frac{\partial}{\partial n}G(P,Q) - 2\beta n_z G(P,Q)\right)\tilde{\phi}(Q)\mathrm{d}S_Q = \int_\Sigma G(P,Q)\frac{\partial}{\partial n}\tilde{\phi}(Q)\mathrm{d}S_Q. \tag{23}$$

In order to obtain the Green's function in Laplace space, Eq. (22) is modified by using the substitution

$$G = \mathrm{e}^{\beta z}v. \tag{24}$$

In this case, the differential equation for the LT space is

$$\nabla^2 v - \left(\beta^2 + \frac{s}{\alpha}\right)v = 0. \tag{25}$$

This equation is the modified Helmholtz equation, whose Green's function is known. Thus the Green's function in 3D

LT space is

$$v = \frac{1}{4\pi r} e^{-\sqrt{\beta^2+(s/\alpha)}\, r}. \tag{26}$$

By back substitution (see Eq. (24)), we obtain

$$G(P,Q,s) = \frac{1}{4\pi r} e^{\beta z} e^{-\sqrt{\beta^2+(s/\alpha)}\, r}. \tag{27}$$

The boundary conditions, Eqs. (5) and (6), must also be transformed into Laplace space, i.e.

$$\begin{aligned} \bar{\bar{\phi}}(Q,s) &= \int_{\mathscr{R}} \bar{\phi}(Q,t) e^{-st}\, dt, \\ \bar{\bar{q}}(Q,s) &= \int_{\mathscr{R}} \bar{q}(Q,t) e^{-st}\, dt, \end{aligned} \tag{28}$$

respectively. For constant boundary conditions, the above equations reduce to (see Brebbia et al. [37], p. 143)

$$\bar{\bar{\phi}}(Q,s) = \frac{\bar{\phi}(Q,t)}{s}, \qquad \bar{\bar{q}}(Q,s) = \frac{\bar{q}(Q,t)}{s}, \tag{29}$$

respectively.

The modified kernel functions, in terms of the Laplace variable s, are

$$G(P,Q,s) = \frac{1}{4\pi r} e^{\beta(z_Q - z_P) - \sqrt{\beta^2+(s/\alpha)}\, r}, \tag{30}$$

and

$$\begin{aligned} \frac{\partial}{\partial n} G(P,Q,s) - 2\beta n_z G(P,Q,s) &= \frac{e^{\beta R_z - \sqrt{\beta^2+(s/\alpha)}\, r}}{4\pi} \\ &\times \left(-\frac{1}{r^2}\frac{\mathbf{n}\cdot\mathbf{R}}{r} - \frac{1}{r}\sqrt{\beta^2 + \frac{s}{\alpha}}\frac{\mathbf{n}\cdot\mathbf{R}}{r} + \frac{1}{r}\beta n_z - \frac{2\beta n_z}{r} \right), \end{aligned} \tag{31}$$

or

$$\begin{aligned} &\frac{\partial}{\partial n} G(P,Q,s) - 2\beta n_z G(P,Q,s) \\ &\quad = -\frac{e^{\beta R_z - \sqrt{\beta^2+(s/\alpha)} r}}{4\pi} \left(\frac{\mathbf{n}\cdot\mathbf{R}}{r^3} + \sqrt{\beta^2 + \frac{s}{\alpha}}\frac{\mathbf{n}\cdot\mathbf{R}}{r^2} + \frac{\beta n_z}{r} \right), \end{aligned} \tag{32}$$

where $\mathbf{n}$ is the unit outward normal at a field point Q, n_z is the z component of $\mathbf{n}$, $\mathbf{R} = \mathbf{Q} - \mathbf{P}$, $R_z = z_Q - z_P$, and r is the norm of $\mathbf{R}$, i.e. $r = \|\mathbf{R}\| = \|\mathbf{Q} - \mathbf{P}\|$.

5. Numerical implementation of the 3D Galerkin BEM

The numerical methods employed in this work use standard Galerkin implementation techniques [30] in conjunction with the LT method. A few aspects of the numerical methods are briefly reviewed in this section.

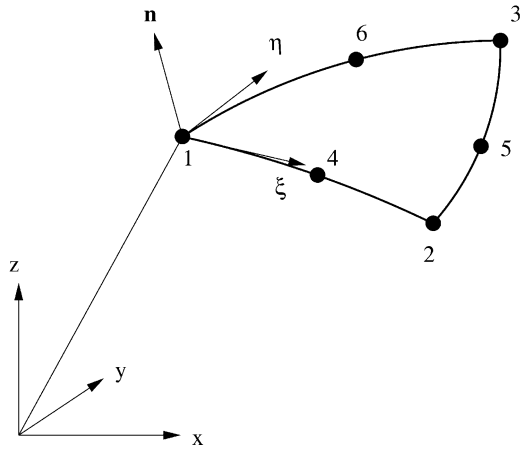

Fig. 1. Isoparametric quadratic triangular element of 6 nodes. The intrinsic coordinate space is the right triangle in (ξ, η) space with $\xi \geq 0$, $\eta \geq 0$ and $\xi + \eta \leq 1$.

5.1. Division of the boundary into elements

The surface of the solution domain is divided into a number of connected elements. Over each element, the variation of the geometry and the variables (potential and flux) is approximated by simple functions. In this study, 6-noded isoparametric quadratic triangular elements are used (see Fig. 1).

The geometry of an element can be defined by the coordinates of its six nodes using appropriate quadratic shape functions as follows

$$x_i(\xi,\eta) = \sum_{j=1}^{6} N_j(\xi,\eta)(x_i)_j. \tag{33}$$

In an isoparametric approximation, the same shape functions are used for the solution variables, as follows

$$\begin{aligned} \phi_i(\xi,\eta) &= \sum_{j=1}^{6} N_j(\xi,\eta)(\phi_i)_j, \\ \frac{\partial \phi_i}{\partial n}(\xi,\eta) &= \sum_{j=1}^{6} N_j(\xi,\eta)\left(\frac{\partial \phi_i}{\partial n}\right)_j. \end{aligned} \tag{34}$$

The shape functions can be explicitly written in terms of intrinsic coordinates ξ and η as follows (see Fig. 1)

$$\begin{aligned} &N_1(\xi,\eta) = (1-\xi-\eta)(1-2\xi-2\eta), \\ &N_2(\xi,\eta) = \xi(2\xi-1), \qquad N_3(\xi,\eta) = \eta(2\eta-1), \\ &N_4(\xi,\eta) = 4\xi(1-\xi-\eta), \qquad N_5(\xi,\eta) = 4\xi\eta, \\ &N_6(\xi,\eta) = 4\eta(1-\xi-\eta). \end{aligned} \tag{35}$$

The intrinsic coordinate space is the right triangle with $\xi \geq 0$, $\eta \geq 0$ and $\xi + \eta \leq 1$.

5.2. Galerkin boundary integral equation

Define

$$\mathscr{B}(P) \equiv \phi(P) + \int_{\Sigma} \left(\frac{\partial}{\partial n} G(P,Q) - 2\beta n_z G(P,Q) \right) \phi(Q) \mathrm{d}S_Q - \int_{\Sigma} G(P,Q) \frac{\partial \phi}{\partial n}(Q) \mathrm{d}S_Q, \tag{36}$$

and thus for an exact solution $\mathscr{B}(P) \equiv 0$.

In a Galerkin approximation, the error in the approximate solution is orthogonalized against the shape functions, i.e. the shape functions are the weighting functions and $\mathscr{B}(P) = 0$ is enforced in the 'weak sense'

$$\int_{\Sigma} N_k(P) \mathscr{B}(P) \mathrm{d}P = 0. \tag{37}$$

After replacing the boundary and the boundary functions by their interpolated approximations, a set of linear algebraic equations emerges

$$[H]\{\phi\} = [G]\left\{ \frac{\partial \phi}{\partial n} \right\}. \tag{38}$$

In computing the matrix elements, the singular integrals must of course be evaluated differently. For Galerkin, there are three distinct situations where singularity must be considered: (a) *Coincident integration case* when P and Q lie in the same element; (b) *Vertex adjacent integration case*, when the vertex is the only common node between two elements; and (c) *Edge adjacent integration case*, when two elements share a common edge. For these situations, a combination of numerical and analytic integration is employed, with the analytic integration based upon a polar coordinate transformation. These techniques are analogous to the two-dimensional methods presented in Ref. [38].

6. Numerical inversion of the Laplace transform

In the LTBEM approach, the numerical inversion of the LT is a key issue. The LT technique has been efficiently applied in conjunction with different numerical methods such as finite difference and finite element methods for the solution of ground water flow and solute transport problems (Sudicky [39], Moridis and Reddell [40]), and heat conduction problems (Chen and Chen [41], Chen and Lin [42]). In these papers, different Laplace inversion algorithms such as those of Talbot [43], Dubner and Abate [44], Durbin [45], Crump [46], and Stehfest [47,48] were used. The advantages and deficiencies of some algorithm were pointed out by Maillet et al. [24]. Davies and Martin [49] made a critical study of the various algorithms. Later, Duffy [50] examined three popular methods for numerical inversion of the Laplace transform, i.e. direct integration [50], Week's method [51] and Talbot's method [43].

As LT inversion is an ill-posed problem, small truncation errors can be greatly magnified in the inversion process, leading to poor numerical results. In recent times, Moridis and Reddell [15] showed that Stehfest's algorithm poses no such problems and high accuracy may be achieved. Subsequently, Zhu et al. [17] and Satravaha and Zhu [18] had similar success using numerical inversion of LT in BEM problems. Recently, Maillet et al. [24] critically reviewed the Stehfest's algorithm and pointed out its advantages and disadvantages. For the present study, a computer code has been written following Stehfest's algorithm [47,48].

The Stehfest's algorithm originates from Gaver [52]. If $\tilde{P}(s)$ is the Laplace Transform of $F(t)$, an approximate value F_a of the inverse $F(t)$ for a specific time $t = T$ is given by

$$F_a = \frac{\ln 2}{T} \sum_{i=1}^{N} V_i \tilde{P}\left(\frac{\ln 2}{T} i \right), \tag{39}$$

where

$$V_i = (-1)^{N/2+1} \sum_{k=(i+1)/2}^{\min(i,N/2)} \frac{k^{N/2}(2k)!}{(N/2-k)!k!(k-1)!(i-k)!(2k-i)!}. \tag{40}$$

Eqs. (39) and (40) correspond to the final form used in our numerical implementation.

When inverting a function from its Laplace transform, one should compare the results for different N, to verify whether the function is smooth enough, to observe the accuracy, and to determine an optimum value of N. Originally, Stehfest suggested to use $N = 10$ for single precision arithmetic; however, Moridis and Reddell [15], and Zhu et al. [17], found no significant change in their results for $6 \leq N \leq 10$. In the present calculations, $N = 10$ was adopted.

Most of the methods for the numerical inversion of the LT require the use of complex values of the LT parameter, and as a result, the use of complex arithmetic leads to additional storage and an increase in computation time. The disadvantage of using complex arithmetic has been overcome in Stehfest's method. It uses only real arithmetic and thus produces significant reduction in storage together with an increased efficiency in computation time.

The second LT technique that has been explored is the method recently developed by Murli et al. [53]. This is a Fourier series method, based on the discretization of the Riemann inversion formula using trapezoidal rule with step size $h = \pi/T$

$$F_N(t) = \frac{\mathrm{e}^{\sigma t}}{T} \mathrm{Re}\left(\frac{F(\sigma)}{2} + \sum_{k=1}^{N} F\left(\sigma + \frac{\mathrm{i}k\pi}{T} \right) \mathrm{e}^{\mathrm{i}k\pi t/T} \right). \tag{41}$$

Compared to Stehfest's algorithm, this method was found to require more iterations to achieve convergence, and moreover requires complex arithmetic. Thus, the results reported below employ the Stehfest's algorithm.

7. Numerical examples

As noted above, the integral equation is numerically approximated via the non-symmetric Galerkin BEM Method. Standard 6-node isoparametric quadratic triangular elements are used to interpolate the boundary geometry and boundary functions for the physical variables. For all the examples, $N = 10$ is used for the Laplace inversion algorithm using the Stehfest's Method (see Section 6).

Five examples are considered:

1. Transient 2D heat conduction in a homogeneous cube.
2. Cylinder with constant surface temperature.
3. Constant temperature on two planes of an FGM cube.
4. Linear heat flux on a face of an FGM cube.
5. Time-dependent boundary condition.

The first two problems deal with homogeneous materials. These problems validate the Galerkin BEM code and ensure that the FGM implementation recovers the homogeneous case when the non-homogeneity parameter β vanishes, i.e. $\beta = 0$. The last three problems deal with transient heat conduction in FGMs, i.e. $\beta \neq 0$. Notice that the prescribed boundary data for the first four problems is time-independent, while for the last problem, it is time-dependent.

7.1. Transient two-dimensional heat conduction in a homogeneous cube

The original version of this problem has been proposed by Bruch and Zyvoloski [54], consisting of a homogeneous two dimensional heat conduction in a square domain, subjected to the following boundary and initial conditions (see Fig. 2(a))

$$\phi(L_x, y, t) = \phi(x, L_y, t) = 1.0 \tag{42}$$

$$\frac{\partial \phi(0, y, t)}{\partial x} = \frac{\partial \phi(x, 0, t)}{\partial y} = 0.0 \tag{43}$$

$$\phi(x, y, 0) = 0.0 \tag{44}$$

where L_x and L_y are the lengths of the solution domain in the x and y directions, respectively. k_x and k_y are the thermal conductivities in x and y directions, respectively, with the specific heat $c = 1.0$. The analytical solution of the 2D problem for temperature [54] is

$$\phi(x, y, t) = 1.0 + \sum_{n=1}^{\infty}\sum_{j=1}^{\infty} C_{nj} \cos\frac{(2n-1)\pi x}{2L_x}\cos\frac{(2j-1)\pi y}{2L_y} \times \exp\left\{-\left(\frac{k_x(2n-1)^2\pi^2}{4L_x^2} + \frac{k_y(2j-1)^2\pi^2}{4L_y^2}\right)t\right\}, \tag{45}$$

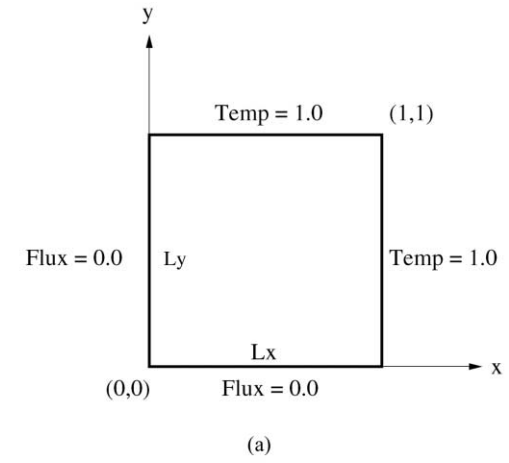

Fig. 2. Geometry and BCs for the cube problem: (a) original 2D problem, (b) equivalent 3D problem. The faces with prescribed temperature (Temp = 1.0) are shaded (example 1).

and the analytical solution for the flux in the y direction is

$$q(x, y, t) = -k_y\frac{\partial \phi}{\partial y} = -k_y\sum_{n=1}^{\infty}\sum_{j=1}^{\infty}\frac{(2j-1)\pi}{2L_y}C_{nj} \times \cos\frac{(2n-1)\pi x}{2L_x}\sin\frac{(2j-1)\pi y}{2L_y} \times \exp\left\{-\left(\frac{k_x(2n-1)^2\pi^2}{4L_x^2} + \frac{k_y(2j-1)^2\pi^2}{4L_y^2}\right)t\right\}, \tag{46}$$

where

$$C_{nj} = \frac{16.0(-1.0)(-1)^{n+1}(-1)^{j+1}}{\pi^2(2n-1)(2j-1)}$$

The 2D problem of Fig. 2(a) is solved using an equivalent 3D problem as shown in Fig. 2(b). The 3D BEM discretization consists of 200 elements on each face of the cube leading to a total of 1200 elements. The flux in the z

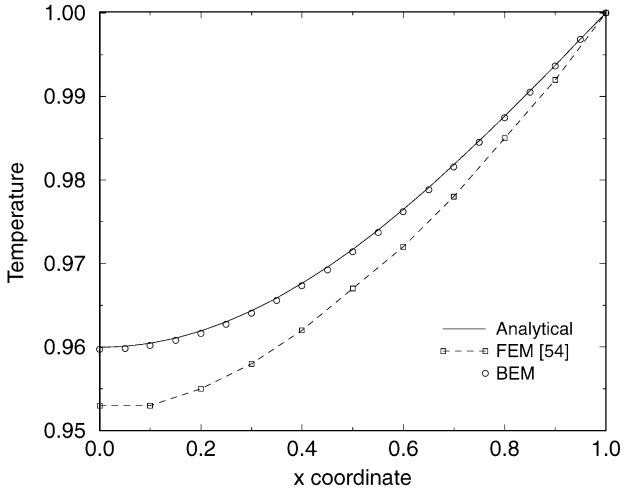

Fig. 3. Temperature variation at edge ($y = 0, z = 1$) (shown with a dark solid line in Fig. 2(b)) considering time $t = 0.75$ for the cube problem with homogeneous material (example 1).

direction is taken as zero to simulate the 2D problem. The cube is analyzed for $0 \le x \le 1.0$, $0 \le y \le 1.0$ with $k_x = k_y = 1.0$. The geometry and boundary conditions of the problem are shown in Fig. 2(b). Fig. 3 shows the variation of temperature at the edge of the top face (shown with a dark solid line in Fig. 2(b)) at $t = 0.75$ considering the present BEM solution, the FEM solution [54], and the analytical solution (Eq. (45)). Note that the BEM solution coincides with the analytical solution within plotting accuracy. Fig. 4 illustrates the variation of temperature at the edge of the top face (shown with a dark solid line in Fig. 2(b)) at different time levels. Again, the BEM solution agrees with the analytical solution within plotting accuracy. Fig. 5 shows the flux distribution along x direction at the $y = 1$ face. The BEM solution and the analytical solution agree quite well.

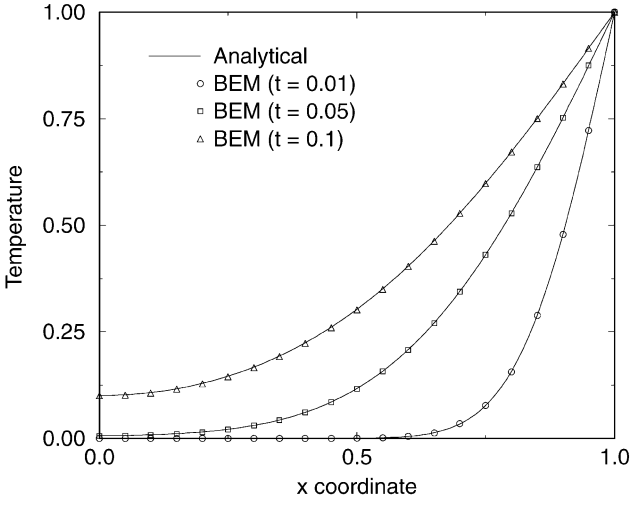

Fig. 4. Temperature variation with distance (x coordinate) (shown with a dark solid line in Fig. 2(b)) at different time levels for the cube problem with homogeneous material (example 1).

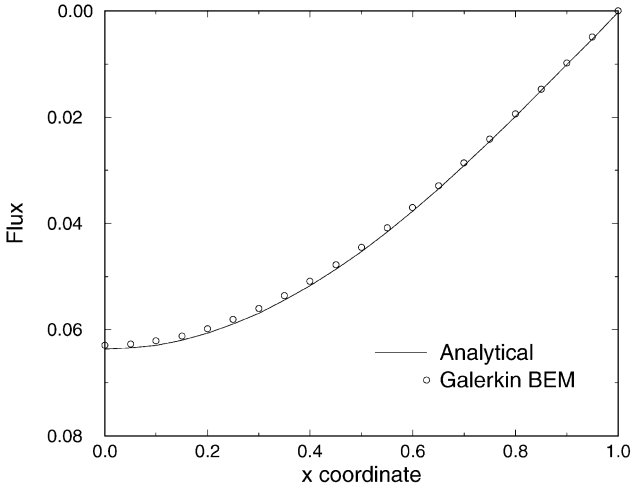

Fig. 5. Flux distribution along x direction at $y = 1$ face for the cube problem with homogeneous material (example 1).

7.2. Cylinder of homogeneous material with constant surface temperature

The second homogeneous test problem involves a cylindrical region, and therefore checks that curved surfaces are being handled correctly. The cylinder has zero initial temperature, the top and the bottom surfaces are insulated, and the wall temperature is kept constant. The geometry and BEM mesh for the cylinder is shown in Fig. 6. The boundary conditions and the initial conditions are as follows:

$$\phi(r,t) = 100, \quad r = 1, \quad r = \text{radial coordinate} \tag{47}$$

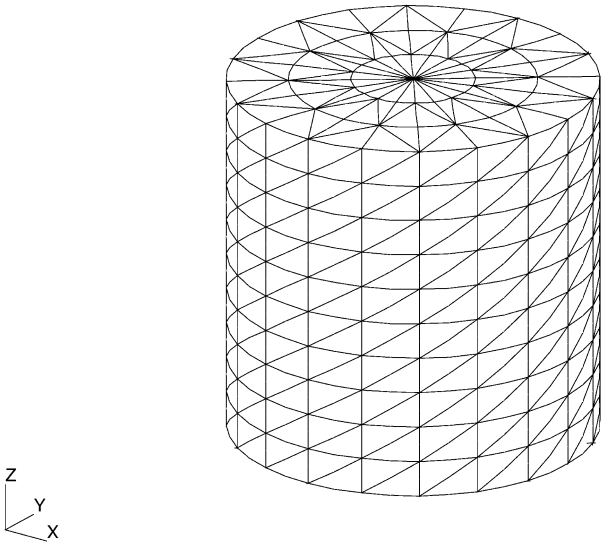

Fig. 6. Geometry and mesh of the cylinder problem (example 2).

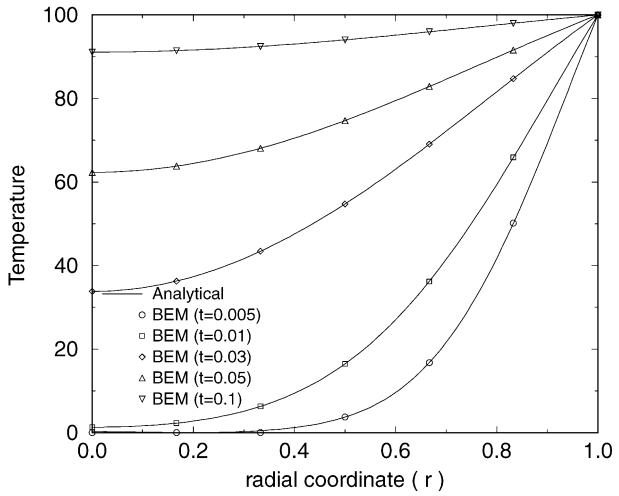

Fig. 7. Variation of temperature along the radial coordinate (r) for the cylinder problem (example 2).

$$\frac{\partial \phi(x,y,2;t)}{\partial z} = \frac{\partial \phi(x,y,0;t)}{\partial z} = 0.0, \tag{48}$$

$$\phi(x,y,z;0) = 0.0 \tag{49}$$

The analytical solution to this problem [31] is

$$\phi = T\left(1 - \frac{2}{a}\sum_{n=1}^{\infty} \mathrm{e}^{-k\alpha_n^2 t}\frac{J_0(r\alpha_n)}{\alpha_n J_1(a\alpha_n)}\right), \tag{50}$$

where T is the surface temperature, a, the radius of cylinder, $k = k_0/c_0$ and $\pm\alpha_n$, $n = 1, 2, \ldots$ are the roots of

$$J_0(a\alpha) = 0. \tag{51}$$

The BEM mesh consists of 600 elements, distributed with 100 elements each for the top and bottom faces, and 400 elements for the cylindrical wall. The variation of the temperature along the radius is plotted on Fig. 7 for various times ($t = 0.005$, 0.01, 0.03, 0.05 and 0.1). Notice that the Galerkin BEM and the analytical results agree within plotting accuracy for all time levels.

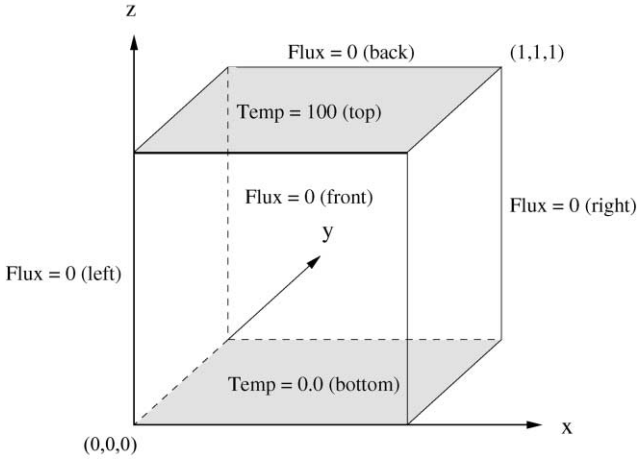

Fig. 8. Geometry and boundary conditions of the FGM cube problem with constant temperature on two planes. The faces with prescribed temperature are shaded (example 3).

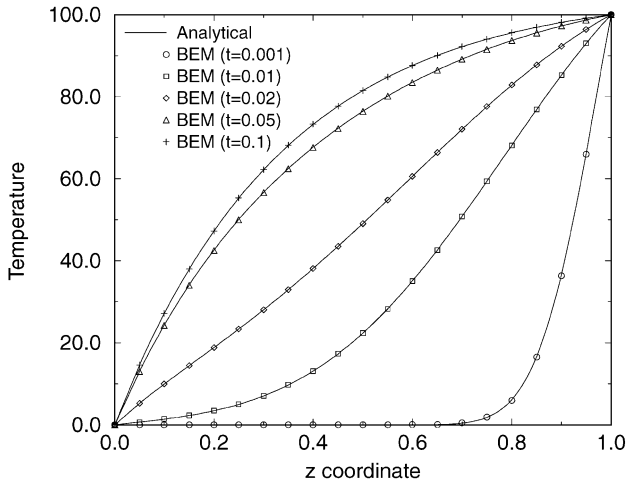

Fig. 9. Temperature profile in z direction at different time levels for the FGM cube problem with constant temperature on two planes (example 3).

7.3. Constant temperature on two planes of a FGM cube

The problem of interest is shown in Fig. 8. The cube initial temperature is zero (see Eq. (7)). Then the top surface of the cube at $[z = 0]$ is maintained at a temperature of $T = 100$, while the bottom face at $[z = 1]$ is zero. The remaining four faces are insulated (zero normal flux). The boundary conditions and the initial conditions are

$$\phi(x,y,0;t) = 0, \quad \phi(x,y,1;t) = 100, \quad \phi(x,y,z;0) = 0. \tag{52}$$

The thermal conductivity and the specific heat are taken to be

$$k(x,y,z) = k_0\mathrm{e}^{2\beta z} = 5\mathrm{e}^{3z}, \tag{53}$$

$$c(x,y,z) = c_0\mathrm{e}^{2\beta z} = 1\mathrm{e}^{3z}. \tag{54}$$

The analytical solution for temperature is (see Appendix A)

$$\phi(x,y,z;t) = \phi_s(x,y,z) + \phi_t(x,y,z;t) = T\frac{1-\mathrm{e}^{-2\beta z}}{1-\mathrm{e}^{-2\beta L}} + \sum_{n=1}^{\infty} B_n \sin\frac{n\pi z}{L}\mathrm{e}^{-\beta z}\mathrm{e}^{-(n^2\pi^2/L^2+\beta^2)\alpha t}, \tag{55}$$

where L is the dimension of the cube (in the z-direction) and

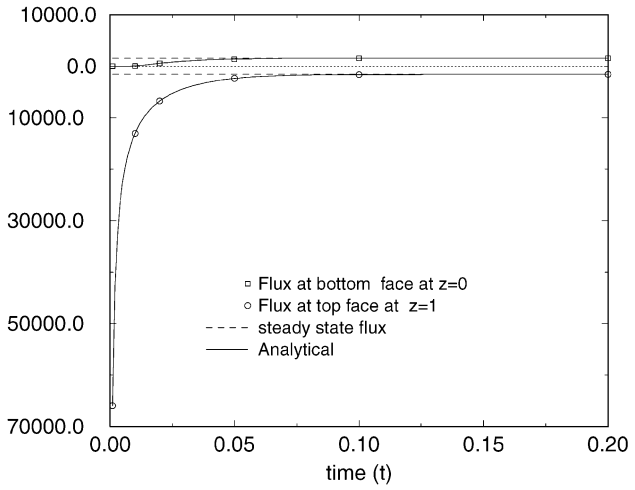

Fig. 10. Change of flux with time for the FGM cube with constant temperature on two planes (example 3).

the analytical solution for flux is (see Appendix A)

$$q(x,y,z;t) = -k(x,y,z)\frac{\partial \phi}{\partial z} = -k(x,y,z) \times \left[\frac{2\beta T \mathrm{e}^{-2\beta z}}{1-\mathrm{e}^{-2\beta L}} + \sum_{n=1}^{\infty} B_n \mathrm{e}^{-\beta z} \mathrm{e}^{-(n^2\pi^2/L^2+\beta^2)\alpha t} \times \left(\frac{n\pi}{L}\cos\frac{n\pi z}{L} - \beta \sin\frac{n\pi z}{L} \right) \right], \quad (56)$$

where

$$B_n = -\frac{2T\mathrm{e}^{\beta L}}{\beta^2 L^2 + n^2\pi^2}\left[\beta L \sin n\pi \frac{1+\mathrm{e}^{-2\beta L}}{1-\mathrm{e}^{-2\beta L}} - n\pi \cos n\pi \right] \quad (57)$$

The Galerkin BEM mesh has 1200 elements with 200 elements on each face. Numerical solutions for the temperature profile at different times are shown in Fig. 9. Notice that the temperature variation matches the analytical solution. Fig. 10 shows the change of flux with time. At the top face, the flux rapidly approaches the steady state flux, while on the bottom face where the temperature is zero; the flux gently approaches to the steady state flux. It is worth observing that the flux from the Galerkin BEM matches the analytical solution of Eq. (56), within plotting accuracy. Finally, a color contour plot of temperatures at $t = 0.5$ is shown in Fig. 11. This plot confirms that the temperature field is one-dimensional and is captured by the Galerkin BEM solution.

7.4. Linear heat flux on a face of a FGM cube

Fig. 12 illustrates a cube that is insulated on the faces $[y = 0]$ and $[y = 1]$, while uniform heat fluxes of 5000 units are added and removed, respectively, at the $[x = 1]$ and $[x = 0]$ faces. In addition, the $[z = 0]$ face is specified to have an x-dependent temperature distribution $\phi = 1000x$ and at $[z = 1]$, a normal heat flux of $q = 15000x$ is removed.

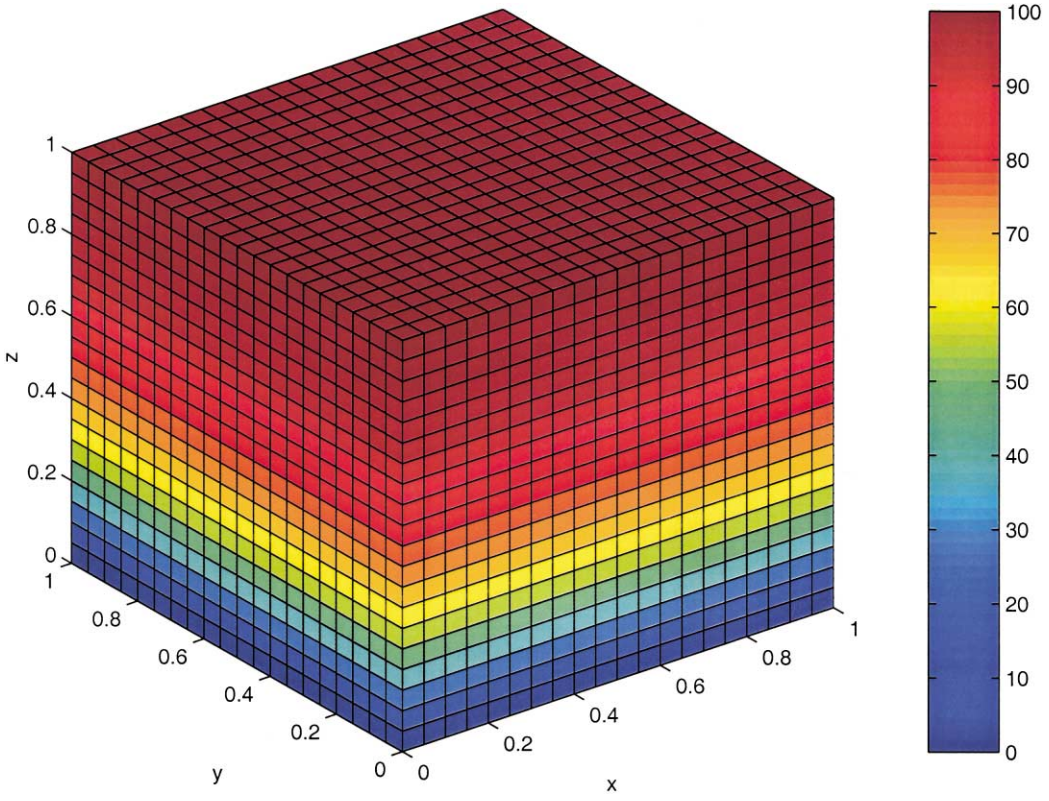

Fig. 11. Color contour plot of temperature at time $t = 0.5$ for the FGM cube with constant temperature on two planes (example 3).

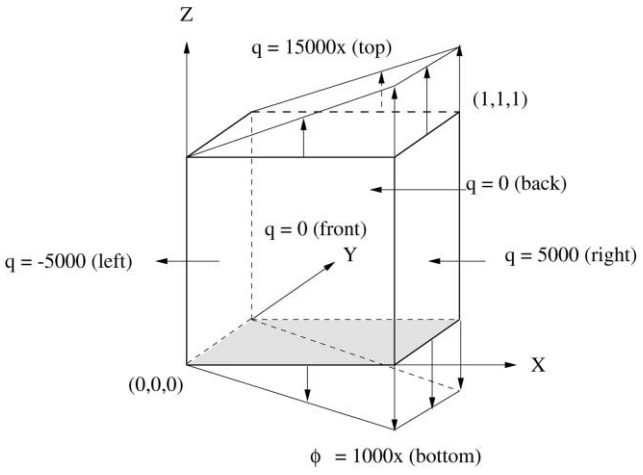

Fig. 12. Geometry and boundary conditions of the FGM cube problem with linear heat flux. The face with prescribed temperature ($\phi = 1000x$) is shaded (example 4).

The initial temperature is zero (see Eq. (7)). The material properties are given by Eqs. (53) and (54). The boundary and the initial conditions for this problem are

$$\phi(x, y, 0; t) = 1000x,$$

$$k(z)\frac{\partial \phi(x, 0, z; t)}{\partial y} = k(z)\frac{\partial \phi(x, 1, z; t)}{\partial y} = 0,$$

$$k(z)\frac{\partial \phi(0, y, z; t)}{\partial x} = -5000, \qquad k(z)\frac{\partial \phi(1, y, z; t)}{\partial x} = +5000,$$

$$k(z)\frac{\partial \phi(x, y, 1; t)}{\partial z} = 15000x, \qquad \phi(x, y, z, 0) = 0. \tag{58}$$

The results of the numerical simulations for the flux distributions along the edge $[y = 0, z = 1]$ for different times are shown in Fig. 13. The exact steady state solution

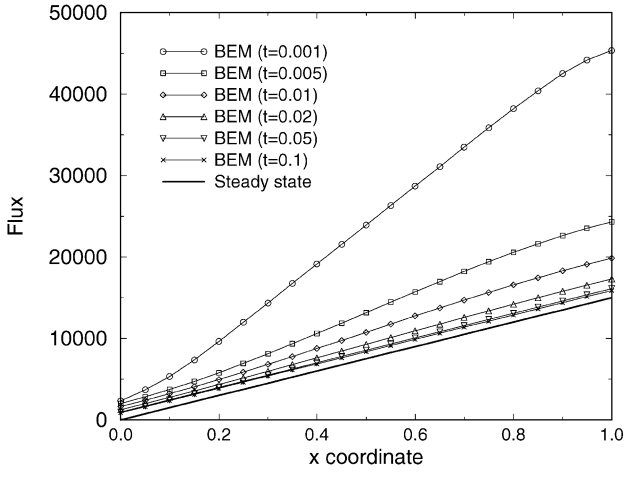

Fig. 13. Flux distribution along edge $[y = 0, z = 1]$ considering various times for the FGM cube problem with linear heat flux in one face (example 4).

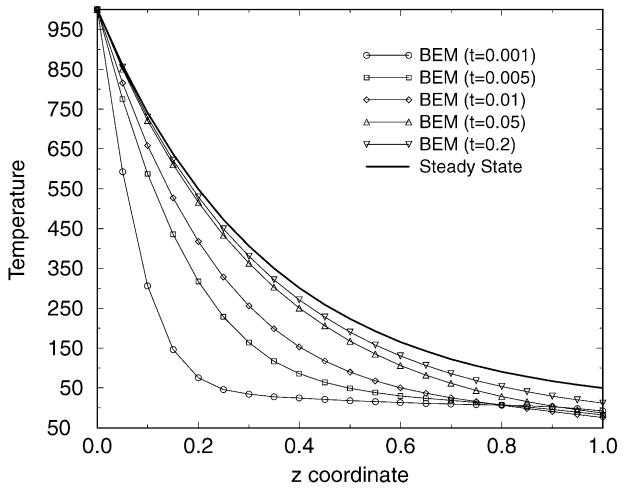

Fig. 14. Temperature distribution along edge $[x = 1, y = 1]$ considering various times for the FGM cube with linear heat flux in one face (example 4).

for flux is

$$k(z)\frac{\partial \phi(x, y, 0, t)}{\partial z} = 15000x. \tag{59}$$

As the time increases, the flux converges to the steady state condition, which is expected.

The temperature distribution along edge $[x = 1, y = 1]$ with various times is plotted in Fig. 14. Notice that as the time increases, the numerical solution approaches the steady state solution, as expected. Finally, a color contour plot for temperature is shown in Fig. 15, for the steady state condition. This plot allows one to verify the 3D surface temperature distribution obtained with the present Galerkin BEM code.

7.5. Time-dependent boundary condition

This problem has prescribed time-dependent boundary condition in one face, while all the other faces are insulated. The top surface of the cube at $[z = 1]$ is prescribed with a time-dependent boundary condition $\phi = 10t$. The material properties are given by expressions (53) and (54). The boundary and initial conditions are

$$\phi(x, y, 1; t) = 10t,$$

$$\frac{\partial \phi(0, y, z; t)}{\partial x} = \frac{\partial \phi(1, y, z; t)}{\partial x} = \frac{\partial \phi(x, 0, z; t)}{\partial y}$$

$$= \frac{\partial \phi(x, 1, z; t)}{\partial y} = \frac{\partial \phi(x, y, 0; t)}{\partial z} = 0, \qquad \phi(x, y, z; 0) = 0 \tag{60}$$

The geometry and boundary conditions are presented in Fig. 16. For the BEM analysis, the same mesh as in the previous example has been used. The temperature profile in the z direction is plotted at $t = 1$ in Fig. 17. In order to compare the results, the problem has been modeled using

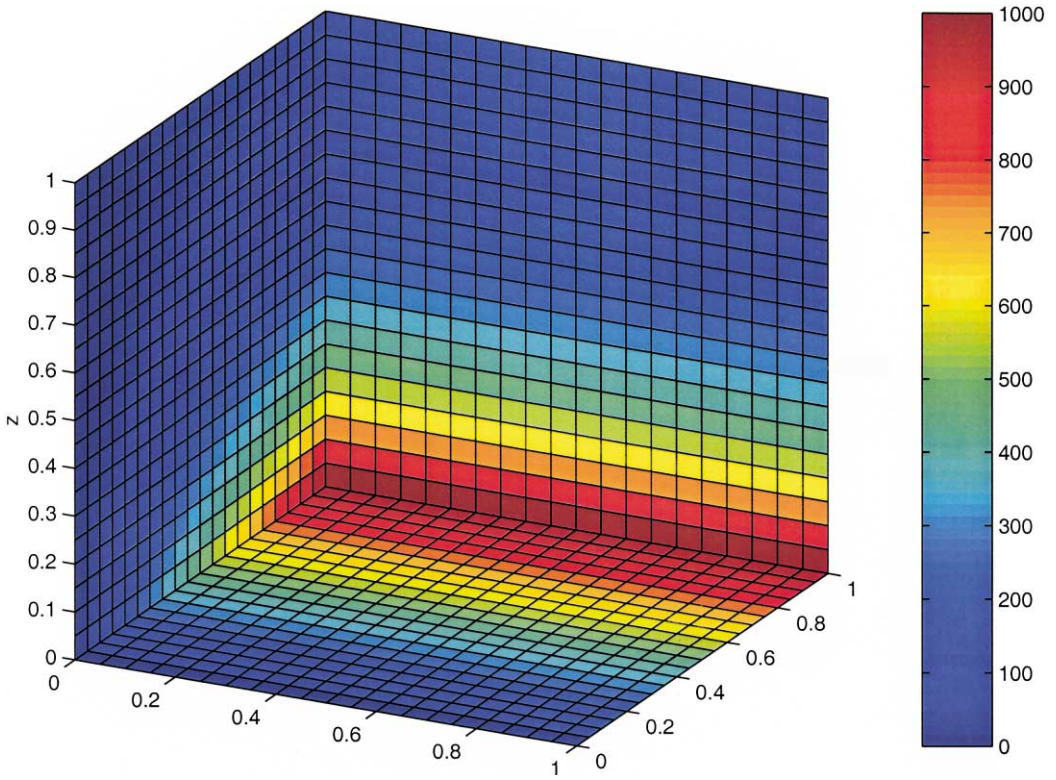

Fig. 15. Color contour plot of temperature at steady state for the FGM cube with linear heat flux in one face (example 4).

commercially available FEM software. The corresponding 2D finite element mesh has 100 linear quadrilateral elements and 121 nodes, the analysis was performed with a time step $\Delta t = 0.01$. From Fig. 17, it is seen that the BEM and FEM results agree well.

8. Conclusions

Boundary element analysis has, for the most part, been limited to homogeneous or piecewise homogeneous media. In this work, it was shown that this method could be successfully applied to analyze transient heat conduction in functionally graded materials, modeled with exponential gradation. In this case, the Green's function can be easily derived using a simple exponential transformation. The presented numerical results based upon this formulation, implemented in a Galerkin BEM framework, agree extremely well with available analytical solutions. The principal computational difficulty with the LTBEM is the numerical inversion of the transform, which was handled accurately and efficiently by Stehfest's algorithm.

Having the boundary integral representation for transient

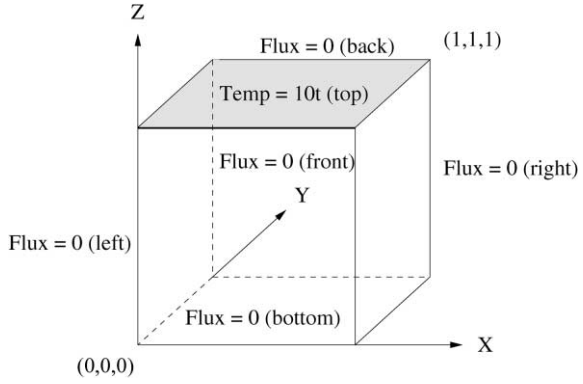

Fig. 16. Geometry and boundary conditions of the FGM cube problem with time-dependent boundary conditions. The face with prescribed time-dependent boundary condition is shaded (example 5).

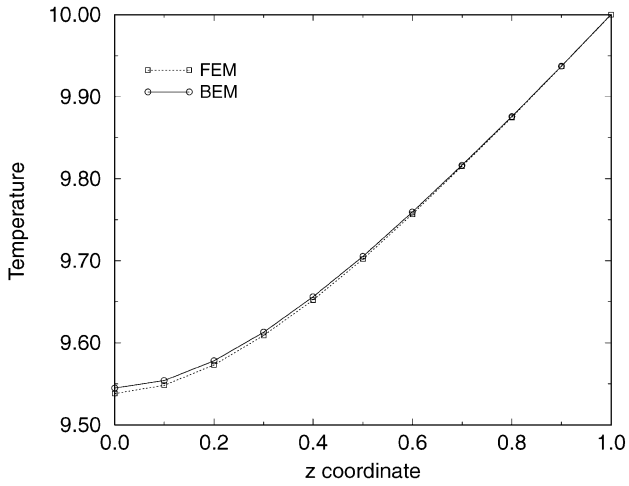

Fig. 17. Temperature profile in z direction at $t = 1$ for the FGM cube problem with time-dependent boundary condition (example 5).

analysis opens the possibility of developing efficient tools for optimization of FGM parameters (e.g. material constants and geometry) and sensitivity analysis [55]. These topics are important for design and application of these new materials.

Acknowledgements

Work at ORNL was supported by the Applied Mathematical Sciences Research Program of the Office of Mathematical, Information, and Computational Sciences, US Department of Energy under contract DE-AC05-00OR22725 with UT-Battelle, LLC. A. Sutradhar acknowledges the support from the DOE Higher Education Research Experience (HERE) Program at Oak Ridge National Laboratory. G.H. Paulino acknowledges the support from the National Science Foundation (NSF) under grant No. CMS-0115954.

Appendix A

A.1. Analytical solution of the FGM cube problem with prescribed temperature on two planes (example 3)

The problem described in Section 7.3 is one dimensional in nature. The governing differential equation is, (cf. Eq. (4))

$$\frac{\partial^2 u}{\partial x^2} + 2\beta\frac{\partial u}{\partial x} = \frac{1}{\alpha}\frac{\partial u}{\partial t}. \tag{A1}$$

The thermal conductivity and the specific heat are taken to be

$$k(x) = k_0 e^{2\beta x}, \qquad c(x) = c_0 e^{2\beta x},$$

and the boundary conditions and initial condition are

$$u(0,t) = 0, \qquad u(L,t) = T, \qquad u(x,0) = 0. \tag{A2}$$

Since the boundary condition of this problem is inhomogeneous and the problem is transient, it is better to express the temperature as the sum of two distributions. One will represent the steady state distribution (independent of t) and the other will represent the transient response. The transient response approaches zero as t increases indefinitely:

$$u(x,t) = u_s(x) + v_t(x,t) \tag{A3}$$

The steady state solution is

$$u_s(x) = T\frac{1 - e^{-2\beta x}}{1 - e^{-2\beta L}}, \tag{A4}$$

and the transient solution is,

$$v_t(x,t) = u(x,t) - T\frac{1 - e^{-2\beta x}}{1 - e^{-2\beta L}}. \tag{A5}$$

This solution will hold for homogeneous boundary conditions. So the modified problem is

$$\frac{\partial^2 v}{\partial x^2} + 2\beta\frac{\partial v}{\partial x} = \frac{1}{\alpha}\frac{\partial v}{\partial t}, \qquad v(0,t) = 0, \qquad v(L,t) = 0 \tag{A6}$$

$$v(x,0) = -T\frac{1 - e^{-2\beta x}}{1 - e^{-2\beta L}} \tag{A7}$$

To solve the problem we use the separation of variables, i.e.

$$v(x,t) = X(x)T(t). \tag{A8}$$

Substituting this assumed form into Eq. (A6) and separating the variables we get

$$\frac{\dfrac{\partial^2 X}{\partial x^2} + 2\beta\dfrac{\partial X}{\partial x}}{X} = \frac{\dfrac{1}{\alpha}\dfrac{\partial T}{\partial t}}{T}. \tag{A9}$$

Thus setting each side of the above equation equal to $-\lambda^2$ leads to

$$\frac{\partial^2 X}{\partial x^2} + 2\beta\frac{\partial X}{\partial x} + \lambda^2 X = 0, \tag{A10}$$

$$\frac{1}{\alpha}\frac{\partial T}{\partial t} + \lambda^2 T = 0. \tag{A11}$$

Now let $X = e^{sx}$ be the solution to Eq. (A10), for which the associated characteristic equation is

$$s^2 + 2\beta s + \lambda^2 = 0 \tag{A12}$$

with

$$s = -\beta \pm i\sqrt{\lambda^2 - \beta^2} \tag{A13}$$

Substituting the value of s we get the general solution

$$X = e^{-\beta x}(A_1 e^{i\sqrt{\lambda^2-\beta^2}x} + A_2 e^{-i\sqrt{\lambda^2-\beta^2}x}). \tag{A14}$$

The term in parenthesis in Eq. (A14) can be rewritten in terms of trigonometric functions, i.e.

$$X(x) = e^{-\beta x}(B_1 \cos\sqrt{\lambda^2 - \beta^2}x + B_2 \sin\sqrt{\lambda^2 - \beta^2}x). \tag{A15}$$

From Eq. (A11), we get the general solution

$$T(t) = Ce^{-\alpha\lambda^2 t}. \tag{A16}$$

Substituting Eqs. (A15) and (A16) in Eq. (A8), we obtain

$$v(x,t) = e^{-\beta x}(A\cos\sqrt{\lambda^2 - \beta^2}x + B\sin\sqrt{\lambda^2 - \beta^2}x)e^{-\alpha\lambda^2 t}. \tag{A17}$$

To satisfy the boundary condition at $x = 0$

$$v(0,t) = 0 = Ae^{-\alpha\lambda^2 t}, \tag{A18}$$

and therefore, A must be zero. To satisfy the boundary

condition at $x = L$

$$v(L,t) = 0 = \mathrm{e}^{-\beta L} B \sin(\sqrt{\lambda^2 - \beta^2}L)\mathrm{e}^{-\alpha\lambda^2 t} \tag{A19}$$

and since $B \neq 0$, we obtain the following equality

$$\sin\sqrt{\lambda^2 - \beta^2}L = 0.$$

This implies

$$\sqrt{\lambda^2 - \beta^2}L = n\pi,$$

or

$$\lambda^2 = \frac{n^2\pi^2}{L^2} + \beta^2, \tag{A20}$$

where $n = 1, 2, 3, \ldots$, so these are the eigenvalues and the associated eigenfunction is

$$v_n = B_n \sin\frac{n\pi x}{L}\mathrm{e}^{-\beta x}\mathrm{e}^{-((n^2\pi^2/L^2)+\beta^2)\alpha t}. \tag{A21}$$

Now by the superposition principle the function v is

$$v(x,t) = \sum_{n=1}^{\infty} B_n \sin\frac{n\pi x}{L}\mathrm{e}^{-\beta x}\mathrm{e}^{-((n^2\pi^2/L^2)+\beta^2)\alpha t} \tag{A22}$$

and B_n will be selected such that it satisfies the initial condition. At $t = 0$, the above expression becomes

$$-T\frac{1 - \mathrm{e}^{-2\beta x}}{1 - \mathrm{e}^{-2\beta L}} = \sum_{n=1}^{\infty} B_n \sin\frac{n\pi x}{L}\mathrm{e}^{-\beta x}. \tag{A23}$$

Recognizing this expression as a half-range expansion of a Fourier sine series, we get

$$B_n = -\frac{2T}{L(1 - \mathrm{e}^{-2\beta L})}\int_0^L (\mathrm{e}^{\beta x} - \mathrm{e}^{-\beta x})\sin\frac{n\pi x}{L}\mathrm{d}x$$

$$= -\frac{2T\mathrm{e}^{\beta L}}{\beta^2 L^2 + n^2\pi^2}\left[\beta L \sin n\pi\frac{1 + \mathrm{e}^{-2\beta L}}{1 - \mathrm{e}^{-2\beta L}} - n\pi\cos n\pi\right]. \tag{A24}$$

Hence, the analytical solution to this problem is

$$u(x,t) = u_s(x) + v_t(x,t) \tag{A25}$$

$$u(x,t) = T\frac{1 - \mathrm{e}^{-2\beta x}}{1 - \mathrm{e}^{-2\beta L}} + \sum_{n=1}^{\infty} B_n \sin\frac{n\pi x}{L}\mathrm{e}^{-\beta x}\mathrm{e}^{-((n^2\pi^2/L^2)+\beta^2)\alpha t}, \tag{A26}$$

and thus the flux is

$$q(x,t) = -k(x)\frac{\partial u}{\partial x} = -k(x)\left[\frac{2\beta T\mathrm{e}^{-2\beta x}}{1 - \mathrm{e}^{-2\beta L}} + \sum_{n=1}^{\infty} B_n \mathrm{e}^{-\beta x}\mathrm{e}^{-((n^2\pi^2/L^2)+\beta^2)\alpha t} \times\left(\frac{n\pi}{L}\cos\frac{n\pi x}{L} - \beta\sin\frac{n\pi x}{L}\right)\right] \tag{A27}$$

where

$$B_n = -\frac{2T\mathrm{e}^{\beta L}}{\beta^2 L^2 + n^2\pi^2}\left[\beta L \sin n\pi\frac{1 + \mathrm{e}^{-2\beta L}}{1 - \mathrm{e}^{-2\beta L}} - n\pi\cos n\pi\right]. \tag{A28}$$

References

[1] Chang Y, Kang CS, Chen DJ. The use of fundamental Green's functions for the solution of problems of heat conduction in anisotropic media. Int J Heat Mass Transf 1973;16:1905–18.

[2] Shaw R. An integral equation approach to diffusion. Int J Heat Mass transf 1974;17:693–9.

[3] Curran DAS, Cross M, Lewis BA. A preliminary analysis of boundary element methods applied to parabolic partial differential equations. In: Brebbia CA, editor. New developments in boundary element methods. Southampton: Computational Mechanics Publications, 1980. p. 179–90.

[4] Wrobel LC, Brebbia CA. The boundary element method for steady-state and transient heat conduction. In: Lewis RW, Morgan K, editors. Numerical methods in thermal problems. Swansea: Pineridge Press, 1979. p. 58–73.

[5] Lesnic D, Elliott L, Ingham DB. Treatment of singularities in time-dependent problems using boundary element method. Engng Anal Boundary Elem 1995;16:65–70.

[6] Coda HB, Venturini WS. A simple comparison between two 3D time domain elastodynamic boundary element formulations. Engng Anal Boundary Elem 1996;17:33–44.

[7] Coda HB, Venturini WS. Further improvements on 3-D treatment BEM elastodynamic analysis. Engng Anal Boundary Elem 1996;17:231–43.

[8] Pasquetti R, Caruso A. Boundary element approach for transient and non-linear thermal diffusion. Num Heat Transf, PartB 1990;17:83–99.

[9] Pasquetti R, Caruso A, Wrobel LC. Transient problems using time-dependent fundamental solutions. In: Wrobel LC, Brebbia CA, editors. Boundary element methods in heat transfer. Southampton, Boston: Computational Mechanics Publications, 1992. p. 33–62.

[10] Divo E, Kassab A. A generalized BEM for steady and transient heat conduction in media with spatially varying thermal conductivity. In: Goldberg M, editor. Boundary integral methods: numerical and mathematical aspects. Southampton, Boston: Computational Mechanics Publications, 1999. p. 37–76.

[11] Wrobel LC, Brebbia CA. The dual reciprocity boundary element formulation for non-linear diffusion problems. Comput Meth Appl Mech Engng 1987;65:147–64.

[12] Nowak AJ. The multiple reciprocity method of solving transient heat conduction problems. In: Brebbia CA, Connor JJ, editors. BEM XI. Computational Mechanics Publications, Springer, 1989. p. 81–95.

[13] Rizzo F, Shippy DJA. Method of solution for certain problems of transient heat conduction. AIAA J 1970;8:2004–9.

[14] Liggett JA, Liu PLF. Unsteady flow in confined aquifers: a comparison of boundary integral methods. Watr Resour Res 1979;15:861–6.

[15] Moridis GJ, Reddell DL. The Laplace transform boundary element (LTBE) method for the solution of diffusion-type equations. In: Brebbia CA, Gipson GS, editors. BEM XIII. Southampton, Boston: Computational Mechanics Publications, 1991. p. 83–97.

[16] Cheng AHD, Abousleiman Y, Badmus T. A Laplace transform BEM for axysymmetric diffusion utilizing pre-tabulated Green's function. Engng Anal Boundary Elem 1992;9:39–46.

[17] Zhu SP, Satravaha P, Lu X. Solving the linear diffusion equations with the dual reciprocity methods in Laplace space. Engin Anal Boundary Elem 1994;13:1–10.

[18] Zhu SP, Satravaha P. An efficient computational method for non-linear transient heat conduction problems. Appl Math Modeling 1996;20:513–22.

[19] Zhu SP. Time-dependent reaction diffusion problems and the LTDRM approach. In: Goldberg M, editor. Boundary integral methods: numerical and mathematical aspects. Southampton, Boston: Computational Mechanics Publications, 1999. p. 1–35.
[20] Goldberg MA, Chen CS. The method of fundamental solutions for potential, Helmholtz and diffusion problems. In: Goldberg M, editor. Boundary integral methods: numerical and mathematical aspects. Southampton, Boston: Computational Mechanics Publications, 1999. p. 103–76.
[21] Cheng AH-D. Darcy's flow with variable permeability: a boundary integral solution. Watr Resour Res 1984;20:980–4.
[22] Wu TW, Lee L. A direct boundary integral formulation for acoustic radiation in a subsonic uniform flow. J Sound Vibr 1994;175:51–63.
[23] Lacerda LA, Wrobel LC, Mansur WJ. A boundary integral formulation for acoustic radiation in a subsonic uniform flow. J Acoust Soc Am 1996;100:98–107.
[24] Maillet D, Andre S, Batsale JC, Degiovanni A, Moyne C. Thermal quadrupoles solving the heat equation through integral transforms. New York: Wiley, 2000.
[25] Gray LJ, Kaplan T, Richardson D, Paulino GH. Green's functions and boundary integral analysis for exponentially graded materials: heat conduction. ASME J Appl Mech 2002 (in press).
[26] Tanigawa Y. Some basic thermoelastic problems for non-homogeneous structural materials. Appl Mech Rev 1995;48(6): 287–300.
[27] Noda N. Thermal stresses in functionally graded material. J Thermal Stresses 1999;22:477–512.
[28] Suresh S, Mortensen A. Fundamentals of functionally graded materials. London: Institute of Materials, IOM Communications Ltd, 1998.
[29] Miyamoto Y, Kaysser WA, Rabin BH, Kawasaki A, Ford RG. Functionally graded materials: design, processing and applications. Dordrecht: Kluwer Academic Publishers, 1999.
[30] Bonnet M. Boundary integral equation methods for solids and fluids. New York: Wiley, 1995.
[31] Carslaw HS, Jaeger JC. Conduction of heat in solids. 2nd ed. Oxford: Clarendon Press, 1959.
[32] Li BQ, Evans JW. Boundary element solution of heat convection–diffusion problems. J Comput Phys 1991;93:255–72.
[33] Ikeuchi M, Onishi K. Boundary elements in transient convective diffusive problems. In: Brebbia CA, Futagami T, Tanaka M, editors. Boundary elements V. Berlin: Springer, 1983. p. 275–82.
[34] Ramanchandran PA. Boundary element methods in transport phenomena. London: Elsevier, 1994.
[35] Singh KM, Tanaka M. On exponential variable transformation based boundary element formulation fro advection–diffusion problems. Engng Anal Boundary Elem 2000;24:225–35.
[36] Partridge PW, Brebbia CA, Wrobel LC. The dual reciprocity boundary element method. Southampton: Computational Mechanics Publications, 1992.
[37] Brebbia CA, Telles JCF, Wrobel LC. Boundary element techniques: theory and applications in engineering. Berlin: Springer, 1984.
[38] Gray LJ. Evaluation of singular and hypersingular Galerkin integrals: direct and symbolic computation. In: Sladek V, Sladek J, editors. Singular Integrals in boundary element methods. Southampton: Computational Mechanics Publications, 1998.
[39] Sudicky EA. The Laplace transform Galerkin technique: a time-continuous finite element theory and application to mass transport in groundwater. Water Resource Res 1989;25:1833–46.
[40] Modiris GL, Reddell DL. The Laplace transform finite difference (LTFD) numerical method for the simulation of solute transport in groundwater. 1990 AGU Fall Meet, San Francisco, EOS Trans Am Geophys Union 1990;71(43).
[41] Chen HT, Chen CK. Hybrid Laplace transform/finite difference method for transient heat conduction problems. Int J Numer Meth Engng 1988;26:1433–47.
[42] Chen HT, Lin J-Y. Application of the Laplace transform to non-linear transient problems. Appl Math Model 1991;15:144–51.
[43] Talbot A. The accurate numerical inversion of Laplace transforms. J Inst Math Appl 1979;23:97–120.
[44] Dubner H, Abate J. Numerical inversions of Laplace transforms by relating them to the finite Fourier cosine transform. J Assoc Comput Mach 1968;15:115–223.
[45] Durbin F. Numerical inversion of Laplace transforms: efficient improvement to Dubner and Abate's method. Computer J 1974;17: 371–6.
[46] Crump KS. Numerical inversion of Laplace transforms using a Fourier series approximation. J Assoc Comput Mach 1976;23:89–96.
[47] Stehfest H. Algorithm 368: numerical inversion of Laplace transform. Commun Assoc Comput Mach 1970;13:47–9.
[48] Stehfest H. Remarks on Algorithm 368. Numerical inversion of Laplace transform. Commun Assoc Comput Mach 1970;13:624.
[49] Davies B, Martin B. Numerical inversion of the Laplace transform: a survey and comparison of methods. J Comput Phys 1979;33:1–32.
[50] Duffy DG. On the numerical inversion of Laplace transforms: comparison of three new methods on characteristic problems from applications. ACM Trans Math Software 1993;19(3):333–59.
[51] Weeks WT. Numerical inversion of Laplace transforms using Laguerre functions. J Assoc Comput Mach 1966;13(3):419–29.
[52] Gaver DP. Observing stochastic processes, and approximate transform inversion. Oper Res 1966;14(3):444–59.
[53] D'Amore L, Laccetti G, Murli A. An implementation of a Fourier series method for the numerical inversion of the Laplace transform. ACM Trans Math Software 1999;25(3):279–305.
[54] Bruch JC, Zyvoloski G. Transient Two dimensional heat conduction problems solved by the finite element method. Int J Numer Meth Engng 1974;8:481–94.
[55] Paulino GH, Shi F, Mukherjee S, Ramesh P. Nodal sensitivities as error estimates in computational mechanics. Acta Mech 1997;121: 191–213.